Published in final edited form as:
Environ Sci Technol. 2011 June 1; 45(11): 4896–4903. doi:10.1021/es104312h.

Dehalogenation of Polybrominated Diphenyl Ethers and Polychlorinated Biphenyl by Bimetallic, Impregnated, and Nanoscale Zerovalent Iron

Yuan Zhuang[a], **Sungwoo Ahn**[b], **Angelia L. Seyfferth**[c], **Yoko Masue-Slowey**[c], **Scott Fendorf**[c], and **Richard G. Luthy**[a,*]

[a]Department of Civil and Environmental Engineering, Stanford University, Stanford, CA 94305-4020

[b]Exponent, Inc., Bellevue, WA 98007

[c]Department of Environmental Earth System Science, Stanford University, Stanford, CA 94305-4020

Abstract

Nanoscale zerovalent iron particles (nZVI), bimetallic nanoparticles (nZVI/Pd), and nZVI/Pd impregnated activated carbon (nZVI/Pd-AC) composite particles were synthesized and investigated for their effectiveness to remove polybrominated diphenyl ethers (PBDEs) and/or polychlorinated biphenyls (PCBs). Palladization of nZVI promoted the dehalogenation kinetics for mono- to tri-BDEs and 2,3,4-trichlorobiphenyl (PCB 21). Compared to nZVI, the iron-normalized rate constants for nZVI/Pd were about 2-, 3-, and 4-orders of magnitude greater for tri-, di-, and mono-BDEs, respectively, with diphenyl ether as a main reaction product. The reaction kinetics and pathways suggest an H-atom transfer mechanism. The reaction pathways with nZVI/Pd favor preferential removal of para-halogens on PBDEs and PCBs. X-ray fluorescence mapping of nZVI/Pd-AC showed that Pd mainly deposits on the outer part of particles, while Fe was present throughout the activated carbon particles. While BDE 21 was sorbed onto activated carbon composites quickly, debromination was slower compared to reaction with freely dispersed nZVI/Pd. Our XPS and chemical data suggest about 7% of the total iron within the activated carbon was zero-valent, which shows the difficulty with in-situ synthesis of a significant fraction of zero-valent iron in the micro-porous material. Related factors that likely hinder the reaction with nZVI/Pd-AC are the heterogenous distribution of nZVI and Pd on activated carbon and/or immobilization of hydrophobic organic contaminants at the adsorption sites thereby inhibiting contact with nZVI.

Introduction

Nanoscale zerovalent iron (nZVI) is an effective reductant for halogenated organic contaminants. Various studies with nZVI have focused on aliphatic contaminants, leaving need to investigate more persistant aromatic contaminants such as polychlorinated biphenyls (PCBs) and polybrominated diphenyl ethers (PBDEs). These halogenated hydrophobic organic contaminants (HHOCs) are recalcitrant and hydrophobic for which sediments serve as a main repository (1, 2). Previous work showed that nZVI alone was ineffective in

*Corresponding author phone: (650) 721-2615; fax: (650) 725-9720; luthy@stanford.edu.

Supporting Information Available
This information is available free of charge via the Internet at http://pubs.acs.org/.

reducing PCBs (3) and PBDEs (4), especially their lesser-halogenated congeners. Palladization of ZVI has been found to improve the rate of dechlorination for chlorinated aromatics, such as PCBs (3), PCDDs (5), and chlorinated benzenes (6). Few reports are available regarding the degradation of brominated aromatics by bimetallic ZVI. Although it was reported that palladium promotes debromination of BDE 47 by microscale zero-valent iron and magnesium (7), data are lacking on the effect of palladium on debromination kinetics and reaction mechanisms for brominated aromatics, including PBDEs.

A reactive nano-Fe/Pd bimetallic system-impregnated activated carbon, termed RAC (Table 1), was described recently for sorption and simultaneous dechlorination of HHOCs, and tested with 2-monochlorobiphenyl in the aqueous phase (8). Hydrophobic organic compounds sorb onto AC strongly (9) and diffuse into AC slowly (10). As palladium is an expensive catalyst, the efficiency of its usage would be an important factor that affects the development of nano-Fe/Pd as a remediation method. Therefore, study of the potential benefits or hindrance effects of impregnation of nZVI/Pd onto activated carbon on dehalogenation reactions are warranted.

In this study, the dehalogenation kinetics and pathways of selected mono- to tri-BDEs and 2,3,4-trichlorobiphenyl (PCB 21) were compared in a series of contact experiments for three types of reductants: nZVI, bimetallic nanoparticles (nZVI/Pd), and nZVI/Pd impregnated activated carbon (nZVI/Pd-AC). The roles of the Pd catalyst, extent of zero-valent iron formation within activated carbon micro-pores, and sorption on activated carbon composites on dehalogenation of PBDEs and PCBs are investigated.

Experimental Section

Synthesis and Characterization of particles

The nZVI was synthesized by aqueous phase reduction of dissolved ferrous sulfate (Fluka) by an excess of sodium borohydride (Sigma-Aldrich) with the method previously reported (4). A solution deposition process was used to palladize wet nZVI. Granular activated carbon (HD 3000, Norit Americas Inc.) larger than no. 30 sieve (0.595 mm) was used as a support for iron. nZVI/Pd-AC particles were synthesized by incipient wetness impregnation of $Fe(NO_3)_3$, $NaBH_4$ reduction, Pd post-deposition with a slight modification from the method previously reported by Choi et al. (8). Details of the synthesis method are described in the Supplemental Information.

The morphology of the iron particles was investigated using transmission electron microscopy (TEM, Tecnai G2 F20 X-TWIN, FEI Company, Hillsboro, OR) with energy dispersive x-ray detector (EDS). The N_2 Brunnaer–Emmett–Teller (BET) specific surface areas of the synthesized particles were measured using a Coulter SA 3100 surface area and pore size analyzer (Coulter Corporation, Miami, FL). The total iron, palladium, and boron contents of the particles were determined from inductively coupled plasma-atomic emission spectrometry (ICP-MS, XSERIES 2, Thermo Scientific, West Palm Beach, FL) by following EPA Method 6010B. The zero-valent iron (Fe^0) content within the particles was determined by acidification and hydrogen reduction as reported in our previous study (4). X-ray photoelectron spectroscopy (XPS, PHI VersaProbe Scanning XPS, Physical Electronics, Inc., Chanhassen, MN) analysis with Al(K) radiation (1486 eV) was performed on the particle surface and after sputtering to survey iron and palladium speciation.

Elemental distributions of Fe and Pd, as well as species distributions of Fe^0 and Fe^{3+} were obtained on a thin section (30 μm) of a nZVI/Pd-AC particle by micro X-ray fluorescence (μXRF) imaging and micro X-ray absorption spectroscopy (μXAS) on beam line 10.3.2. at

the Advanced Light Source at Lawrence Berkeley National Laboratory, after embedment in epoxy (EPO-TEK 301 2FL). (See Supporting Information.)

Dehalogenation Experiments

Debromination tests by nZVI, nZVI/Pd, and nZVI/Pd-AC on the selected PBDEs (Accustandard) and PCB 21 (Ultra scientific) were conducted to investigate the dehalogenation pathways and reaction kinetics. The PBDE and PCB stock solutions (around 250 μg/L) were prepared in an acetone/milli-Q water solution (50:50, v/v, pH=7) with 0.4% sodium azide (Fisher) added to minimize microbial degradation. Dehalogenation experiments were conducted either in ambient conditions without precautions to exclude oxygen or under anoxic conditions where stock solutions were purged with N_2 to reduce dissolved oxygen levels to around 0.5 ppm. One g of nZVI, 0.1 g of nZVI/Pd or 0.1 g of synthesized nZVI/Pd-AC material was added to a 40 mL vial containing 10 mL of the individual PBDE or PCB stock solution. The sample vial was capped with Teflon septa, placed on a horizontal shaker at 60 rpm, and covered to avoid photodegradation. All samples were prepared in triplicate. Blank samples without contaminants but using the same solvent were set up in the same way for nZVI and nZVI/Pd. At preselected time intervals, samples were sacrificed to measure headspace H_2, and the concentrations of the parent compound as well as the reaction products.

The whole nZVI and nZVI/Pd samples were extracted three times using 3 mL toluene (for PBDEs) or hexane (for PCB 21). For nZVI/Pd-AC tests, PBDE concentrations in the liquid phase and solid phase were measured separately. PBDE and PCB samples were determined as described previously via gas chromatography with mass spectrometric detector (GC-MSD) (4) and gas chromatography with electron-capture detector (GC-ECD) (1). Details on sample extraction and GC analysis are available in the Supporting Information.

Results and Discussions

Particle Characterization

The particle size, specific surface area and the chemical compositions of nZVI, nZVI/Pd, and nZVI/Pd-AC obtained with TEM, ICP-AES and H_2 analyses are given in Table 1. The majority of the synthesized nZVI/Pd particles were about 20 – 50 nm in diameter as determined from TEM images (Figure S1) and were smaller than that of the nZVI (50–70 nm). Somewhat variable particle sizes result from differences in synthesis conditions, including pH, mixing intensity, and palladization processes. Such size distributions with comparable BET specific surface areas have been reported in studies that employed similar synthesis methods (3, 6, 11). The main oxide form of iron was Fe_2O_3 based on XPS analysis for both nZVI (4) and nZVI/Pd. Isolated Pd particles were not observed with TEM imaging, indicating that the Pd additives were heterogeneously distributed on the iron surface as a sparse layer of Pd atoms by this solution deposition process (12).

It was hypothesized that the mesoporous structure in HD3000 GAC would be a good candidate for nZVI/Pd impregnation. The impregnation of nZVI and Pd onto HD3000 decreased both the BET specific surface area and the total pore volume. Following a similar synthesis procedure described by Choi et al. (8), the nZVI/Pd-AC particles have a satisfactory loading of total iron of about 14% by weight. However, elemental analysis by acidification and hydrogen evolution showed that only around 7% of the total iron is Fe^0. The Fe 2p3 spectra from XPS (Figure S2(a)) shows a strong signal of Fe^{3+} (mainly Fe_2O_3) on the surface of the particles that might form from the oxidation by Pd^{2+} or during the vacuum freeze drying process. Although some $Fe(OH)_3$ may have been transformed to Fe_2O_3 via dehydration under the m oderately high vacuum of the XPS, the Fe^0 is observed

by spectra peaks at 706.9 eV (Fe $2p_{3/2}$) and 719.9 eV (Fe $2p_{1/2}$) up to a depth of 75 nm by Ar^+ sputtering. From μXRF images of iron species distributions on a thin section through a nZVI/Pd-AC particle (Figure 1), Fe^{3+} can be found across the whole particle with some holes caused by physical voids or pore blocking, whereas Fe^0 is in very low abundance, which agrees with the chemical analysis at about 1% of total particle weight. Efforts taken to increase Fe^0 loading, such as increasing impregnation time and increasing the amount of borohydride, were unsuccessful. The Pd 3d region of the XPS spectra (Figure S3) includes only two peaks at binding energies of 340.3 eV (Pd $3d_{3/2}$) and 335.0 eV (Pd $3d_{5/2}$), indicating that Pd^{2+} is reduced to Pd^0. Moreover, as shown in Figure 1(b), Pd mainly is deposited on the outer part of nZVI/Pd-AC particles as it encounters iron near the outer surface. Therefore, limited quantities of Fe^0 were in contact with Pd and would not contribute directly to catalytic reduction of halogenated compounds.

Kinetics of PBDE Debromination by nZVI/Pd

In ambient conditions, nZVI/Pd with 0.37 w/w% Pd loading, can debrominate selected mono- to tri-BDEs, including BDE 1, 2, 3, 8, 12, 21, 28, 33, to a low level within 1 day (Figure S4). A pseudo-first-order kinetic model (Equation S1) was assumed to describe the reductive reaction of PBDEs by nZVI/Pd. Standard linear regression was used to obtain k_{obs} values shown in Table 2. The rate of debromination of the PBDEs was increased greatly by palladium. Compared to rates observed with nZVI in our previous study, the iron normalized rate constants, k_{Fe}, by nZVI/Pd were almost 2, 3, and 4 orders of magnitude greater for tri-, di-, and mono-BDEs, respectively.

In accord with findings from PBDE debromination by nZVI in our previous study (4) and micro-ZVI (13), the observed rate constants by nZVI/Pd decrease with fewer number of bromines, but to a much smaller extent. While almost ten times difference in debromination of mono- to tri-BDEs by nZVI was observed for adjacent homologues, this was reduced to within a factor of two for debromination by nZVI/Pd. Lowest unoccupied molecular orbital energies (E_{LUMO}) and heat of formation (H_f) were used as descriptor variables to correlate with k_{obs} for selected mono- to tri-BDEs by nZVI/Pd and nZVI (Figure S5). Both linear fittings for nZVI/Pd are level and have much lower R^2 values (0.129 for H_f and 0.128 for E_{LUMO}) than for nZVI (0.854 for H_f and 0.692 for E_{LUMO}), indicating a weak correlation between catalyzed rates and E_{LUMO} or H_f. Profound changes in structure-activity relationships between zero-valent metal and palladized zero-valent metal were observed also for dechlorination of PCB with Pd/Fe (3) and Pd/Mg (14), and PCDDs with nZVI/Pd (5). Such level free energy relationships are evidence that precursor complex formation (including mass transfer) rather than electron transfer is rate controlling (15).

Debromination tests for BDE 8, 12 and 33 by nZVI/Pd conducted under anoxic conditions (O_2 = 0.5 ppm) revealed a faster debromination process than for tests conducted under ambient conditions (O_2 = 7.8 ppm). Procedures to exclude oxygen increases corresponding observed rate constants 3–4 times (Table 2). Similarly, the efficiency of chloroform degradation by ZVI/Pd increased 2–4 times with solutions bubbled with O_2, air, and N_2 (16). Oxygen should oxidize iron particles (Equation 1) and compete with debromination, as well as water reduction which generates H_2 on the Pd or Fe surface (Equation 2).

$$Fe^0 + \frac{1}{2} O_2 + 2 H_2O \rightarrow Fe^{2+} + H_2O + 2 OH^- \quad \text{(Eq. 1)}$$

$$Fe^0 + 2H_2O \rightarrow Fe^{2+} + H_2 + 2 OH^- \quad \text{(Eq. 2)}$$

Both iron corrosion and reduction reactions contribute to an increase of pH. The pH for debromination tests increased from 7 to 9.5 in one day, and gradually increased to 10 in twenty days (Figure S6). It was reported that dechlorination kinetics of PCB 1 by Pd/ZVI only decreased slowly in the mid range of pH (5.5–9.5), and decreased faster in the upper range of pH (9.5–12.5) (17). It was also found that the debromination of BDE 209 by nZVI decreased slowly, within a factor of two, with increasing pH from 5 to10 (18). Therefore, such change in pH would explain the slower BDE degradation by nZVI/Pd at the later reaction stage (6–24 hours).

In this study, measurement of headspace H_2 as a function of time was used as a metric for the rate of water reduction. A near linear increase of H_2 concentration was detected over 50 days for nZVI tests and 7 days for nZVI/Pd tests. Thus, an average H_2 production rate can be obtained for each case as shown in Table 3. It was observed that these rates did not differ with the presence of PBDEs because of the low concentration of PBDE in solution. For nZVI/Pd and nZVI tests, the involvement of O_2 decreases H_2 production by 15–20%, which was much more than the loss of H_2 production due to the reaction shown in Eq. 1. This phenomenon might be attributed to passivation of Fe^0 by oxygen through the formation of an Fe^{3+} (hydr)oxide surface precipitate.

An enhanced rate of iron corrosion is consistent with the formation of a galvanic couple between Pd and Fe (19). The amount of O_2 (0.2 – 2.5 μmol) and PBDEs (~0.06 μmol) in the system is minimal, compared with Fe^0 (1 mmol) and the daily evolution of H_2 in the system (0.2 mmol), to attribute to iron corrosion without production of H_2 as indicated in Eq. 1. Therefore, production of H_2 can be a good indicator for iron corrosion to examine the metal additives' influence on the formation of active galvanic couples. Galvanic coupling between the iron and the noble metal accelerates contaminant reduction by electron transfer (20), and it also favors water reduction and formation of activated H-species, which in turn can contribute to increased rates of contaminant reduction (11, 19). The relative significance of electron transfer versus hydrogen atom transfer has long been debated as to why palladized iron often shows faster kinetics for contaminant reduction. In our study, the rate of H_2 production by water reduction for nZVI/Pd was two orders of magnitude greater compared to that for nZVI. Since the nZVI/Pd increased the k_{Fe} values for mono-, di-, and tri-BDEs by 4, 3, 2 orders of magnitude, respectively, galvanic couple formation could not account for the whole portion of the rate enhancements for PBDEs in our nZVI/Pd system. The ambient conditions reduced debromination rates by 3–4 times compared with anoxic conditions, and reduced H_2 production by only 15–20%. Therefore, activated H-species on the Pd surface or different "active" reductants might play some role in accelerating rates for PBDE reduction, probably via nucleophilic attack at a halogen substituent (19).

Debromination Pathways of PBDEs by nZVI/Pd

With nZVI/Pd, PBDEs were debrominated to their lower brominated intermediates and diphenyl ether (DE), the completely debrominated form of PBDEs (Figure S4). The main reaction product for mono-BDEs was DE, which showed a mass balance with corresponding loss of the parent mono-BDE. In the case of selected di-BDEs and tri-BDEs, the main products are DE and BDE 1, if the parent BDE has bromine on the ortho position. All the other identified intermediates account for less than 10% of the total mass balance. Besides enhanced kinetics, palladium shows obvious effects on the debromination pathways. For example, the main debromination pathway of BDE 21 by nZVI/Pd was (Figure S4(a)) 2,3,4-triBDE → unknown di-BDE → 2-monoBDE → DE, while reaction by nZVI showed 2,3,4-triBDE → 2,4-diBDE → 4-monoBDE → DE (4). The main debromination pathway of BDE 28 by nZVI/Pd was 2,4,4'-triBDE → 2,4'-diBDE → 2-monoBDE → DE, while reaction by nZVI was 2,4,4'-triBDE → 4,4'-diBDE (13). These changes of pathways further indicate that the dominant debromination reaction takes place on the surface of palladium, where

electron transfer is not the dominant mechanism as it is for uncatalyzed zero valent metals with PBDEs (13), PCDDs (5), and PCBs (21).

A degradation model following sequential debromination reactions cannot fully explain the instant formation of DE in the beginning of the reaction for tri- and di-BDEs, indicating that a concerted (i.e., simultaneous) pathway was involved as suggested in the Supporting Information (Equation S2–S3 and Figure S7). Unlike unpalladized ZVI (4), palladized ZVI promotes concerted debromination universally where no adjacent bromines exist. Nevertheless, the existence of adjacent bromines benefits concerted pathways as more DE is formed initially for BDE 12 compared with BDE 8, and for BDE 33 compared with BDE 28. Kim et al. (22) also concluded from dechlorination of di-PCBs by Pd/Fe that a concerted reaction occurred simultaneously with stepwise reactions. Therefore, it is worthwhile noting that the degradation pathway is both compound specific and reductant specific. Concerted dehalogenation reactions induced by palladium would promote the debromination of PBDE to proceed further and reduce overall toxicity of transformation products.

We observed from debromination tests with mono-BDEs that the susceptibility of bromine for debromination by nZVI/Pd follows the order of para-, meta-, and ortho-position. The persistence of ortho-bromine is remarkable throughout our debromination tests on selected BDEs, including BDE 8, BDE 21, BDE 28, and BDE 33. For the case of BDE 12, it was clear that the para-bromine undergoes the debromination preferentially, resulting in less BDE 3. Such positional preference is different from BDE debromination by ZVI, where meta-bromine is the most susceptible (4, 13) and para-bromine is the most persistent (13, 23). This notable effect of palladization on the pathway of debromination can be explained by steric considerations, where a steric hindrance could inhibit the formation of any precursor complex between the H atom and PBDEs, the same as that indicated for PCBs (24). The ortho-bromines are most hindered by neighboring oxygen, while para-bromines bear the least hindrance from the oxygen atom and the other phenyl ring. Although the toxicity of PBDEs is not as fully studied as for PCBs and PCDDs, fast and preferred elimination of para-bromines by nZVI/Pd would likely reduce their estrogenic potencies (25, 26), while the preferential removal of meta-bromine by nZVI would not.

Mass balances were calculated to consider any possibility of irreversible sorption or non-extractable compound formation. The recoveries were satisfactory for mono- and di-BDEs studied (90–100%), while recoveries for tri-BDEs (BDE 21, 28 and 33) were lower (7085%). Among the same homologue, those BDEs with adjacent bromines (BDE 12, 21 and 33) showed a lower recovery by nZVI/Pd, which is consistent with what we observed for the case of nZVI. This indicates that the chance of forming other degradation compounds with nZVI/Pd by other transformation mechanisms was greater for higher-brominated diphenyl ethers, especially for those with adjacent bromines. Efforts were made to prove the existence of unknown intermediates with available analytical methods, but none of those products were identified.

Dechlorination of PCB 21 by nZVI and nZVI/Pd

PCB 21 (2,3,4-trichlorobiphenyl) dechlorination tests by 1 g nZVI and 0.1 g nZVI/Pd with 0.25 w/w% Pd loading were conducted for 20 days and 70 days, respectively. Pseudo-first-order kinetics were assumed to obtain the rate constants normalized by the amount of iron, k_{Fe}, and palladium, k_{Pd} (Table 2). The half-life of PCB 21 by nZVI alon e was found to be 1 year even under conditions with excess nZVI, indicating the necessity of introducing a noble metal (e.g., Pd) to enhance the corrosion of the reactive metal (e.g., Fe) for reaction with the PCB. By comparing the nZVI content normalized rate (k_{Fe}), palladization was found to increase the rate of dechlorination for PCB 21 by 500 times, which was greater than the increase of the H_2 production rate. Therefore, galvanic couple formation could not account

for the whole portion of the rate enhancements for PCB 21 in our nZVI/Pd system. PCB 21 reduction was 100 times slower than BDE 21 by either nZVI or nZVI/Pd. The ease of reductive dehalogenation follows the bond dissociation energy, C-Br (67 kcal/mol) versus C-Cl (81 kcal/mol) (27), which holds also for liquid phase dehalogenation of halogenated methanes using nZVI/Pd (28).

For both nZVI and nZVI/Pd, the only PCB transformation product detected was PCB 5 (2,3-dichlorobiphenyl), the product of dechlorinating para-chlorine from PCB 21, and a good mass balance was obtained (Figure S8). This preference of para- elimination is consistent with reports of PCB dechlorination by ZVI (3, 29), Pd/Fe (22), Pd/Zn (22) and Pd/Mg (14). No obvious accumulation of mono-PCB and biphenyl was observed during the test, indicating slower dechlorination of PCB 5 than PCB 21 and no apparent concerted pathway under our experimental conditions. The susceptibility of para-chlorines indicates that more toxic “coplanar” PCB congeners were easily reduced. The difference in positional preference by nZVI between PCBs and PBDEs might be caused by the oxygen atom between the two rings which acts as an activator to meta-halogens. Steric hindrance might be the key factor that contributes to the tenaciousness of ortho-halogens on both PCBs and PBDEs by nZVI/Pd (14).

Dehalogenation by nZVI/Pd-AC

Data in Figure S9(a) show the mole fraction of BDE 21 remaining in the aqueous phase and extracted from the solid phase over time. The fraction of BDE 21 in the aqueous phase decreases dramatically in two days, while the fractions of BDE 21 and its debrominated products increase in the solid phase. But no obvious change in solid phase BDE was observed after five days, indicating sorption without further debromination. Due to the strong sorption of BDEs on activated carbon, the total recovery from the solid is around 70% using the soxhlet technique, which was found to be the most efficient extraction method in our study. To complete the mass balance, it was assumed that the percentage of each compound in the unextracted portion of solid phase is the same as that observed from the extracted portion, resulting in Figure S9(b). Similar to debromination of BDE 21 by nZVI/Pd, an unknown di-BDE, BDE 1 and DE were the main products as shown in Figure S9(c). BDE 7 and 5/12 were the main products for debromination of BDE 21 by nZVI and contribute to a greater fraction in the products than that detected in the debromination tests by nZVI/Pd, indicating that BDE 21 was reduced by both nZVI/Pd and nZVI impregnated in AC. The μXRF image in Figure 1(b) shows that palladium is distributed mainly on the outer surface and heterogeneously with iron, leaving much of the iron independent of Pd. Thus BDE 21 could be debrominated on either nZVI or the Pd surface by chance as it diffuses to those active sites within nZVI/Pd-AC particles.

To study the kinetics of the debromination by nZVI/Pd-AC, a general mechanism for the surface reaction on nZVI/Pd impregnated in AC is proposed to proceed via a sequence of individual steps, considering the structure of activated carbon: (1) diffusion of reactants through the solid-liquid boundary layer to the exterior of the particles; (2) diffusion of reactants into the pore network of the particle and association with an active site on the surface; (3) chemical reaction between reactants and active sites on the particle; and (4) desorption and diffusion of products out of the particle. In the experimental setup of this study, step (1) is minimized by complete mixing, and can be measured by the sorption of BDE 21 from the aqueous phase to the solid phase; steps (2) and (3) are controlled by the distribution of ZVI and Pd and the kinetics of reaction; and step (4) is determined by desorption kinetics, which is negligible because there was no accumulation of products in the aqueous phase. The simplified scheme of the whole process is shown in Figure S10, wherein debromination occurs after BDE is sorbed onto the solid phase.

Due to high adsorptive capacity of AC (K_{AC}) and initial low concentration of BDE 21, the depletion of BDE 21 from the liquid phase approximately follows first-order sorption kinetics with rate constant "k_a" (Equation 3), which was fitted to be 3.13 day^{-1}. The change of Fe^0 content by reacting with solution (water: acetone 50/50 w/w) was tested (Figure S11). A first-order rate constant, "k_w", was determined to be 0.29 day^{-1} (i.e., Equation 4). The theoretical H_2 production rate under ambient conditions resulting from the loss of Fe^0 in 1 day was found to be similar to that of nZVI/Pd (3500 mmol/kg Fe^0/d), but slowed afterward, indicating that the remaining nZVI was not as reactive probably because it is not in contact with Pd or sheltered by the pores of AC and an oxide layer. Considering the significant loss of Fe^0 content within ten days, the debromination reaction was assumed to be second-order with respect to both BDE and Fe^0 content, and represented by Equations 3 to 6. Equation 3 is the rate expression for sorption onto AC and Equation 4 is the rate of reaction of nZVI with water and oxygen in the system. Equation 5 expresses the change of BDE 21 in the solid phase, including incoming by sorption and disappearance by debromination. Equation 6 expresses the change of Fe^0 content, including reaction with water and with BDEs. Inputting "k_a" and "k_w" to Eq. 5 and 6, a numerical method in Matlab was used to estimate "k_r", as shown in Figure S12. The model captured the change of BDE 21 in the solid phase well, including the initial increase due to sorption, the decrease due to debromination, and the final level due to the inactivity of ZVI in the system. The resulting Fe^0 content normalized rate k_r, and corresponding first-order rate k_{obs} and Pd content normalized rate k_{Pd} values are summarized in Table 2.

$$\frac{dC_{BDE}^{Aq}}{dt} = -k_a\left(C_{BDE}^{Aq} - \frac{C_{BDE}^{S}}{K_{AC}}\right) \approx -k_a C_{BDE}^{Aq} \quad \text{(Eq. 3)}$$

$$\frac{dC_{nZVI}^{w}}{dt} = -k_w C_{nZVI}^{w} \quad \text{(Eq. 4)}$$

$$\frac{dF_{BDE}^{S}}{dt} = -k_a e^{-k_a t} - k_r C_{nZVI} F_{BDE}^{S} \quad \text{(Eq. 5)}$$

$$\frac{dC_{nZVI}}{dt} = -k_w C_{nZVI} - k_r C_{BDE}^{0} F_{BDE}^{S} C_{nZVI} \quad \text{(Eq. 6)}$$

The rate k_r for the nZVI/Pd-AC test was controlled by the kinetics of reaction as well as the distribution of ZVI and Pd. During the period of tests, pH increased from 7 to around 7.5, and thus was not expected to affect the reaction kinetics. In comparing the reaction kinetics, the Pd content normalized rates, k_{Pd}, for two particles, nZVI/Pd and nZVI/Pd-AC, should be similar because same amount of particles with similar Pd loading were applied in the tests and Pd was the main reaction surface due to its fast kinetics. Therefore, the forty-eight times difference between k_{Pd} for the two particles indicates factors related to the differences in the amount of Fe^0, and the availability of Pd, ZVI, and BDE for the reaction. For nZVI/Pd-AC, only 1% by weight is zero-valent iron and also not all the BDE may be freely available for reaction due to the strong sorption and slow diffusion on the AC surface. In addition, the heterogeneous distribution of Pd and ZVI might contribute to the inactivity and unavailability of Pd and ZVI surfaces.

The small loading of Fe^0 in our study and its inactivation overtime contributed to the uncertainty of kinetic comparison. To further investigate the effect of nZVI/Pd impregnation on AC, data on the dechlorination of PCB 21 by RAC reported by Choi et al. (30) are summarized in Table 2. The dominant iron oxide form reported by Choi et al. was found to be Fe_2O_3 by TEM imaging (8). The amount of Pd on RAC is a limiting factor for reaction, because a linear increase in the reactivity of RAC on PCB 1 dechlorination with Pd loading (0.01~5%) was reported (30). The solution pH was unbuffered in Choi's study and increased to 8–9, which is not expected to affect the rate of dechlorination significantly (31). Thus, the Pd-content normalized rate constants k_{Pd} (Table 2) would be a reasonable parameter to compare the dehalogenation kinetics of PCB 21 by nZVI/Pd and RAC reported by Choi et al (30). Faster kinetics would be expected for dechlorination of PCB 21 by nZVI/Pd under anoxic conditions and without increase in pH from 7 to 10. Therefore, the six times difference between k_{Pd} for nZVI/Pd under ambient conditions and RAC under anoxic conditions would confirm the retarding effect of AC on the rate of dehalogenation. This is caused by the lesser availability of Pd, ZVI, or BDE and leads to less efficient usage of Pd. Still, sorption of AC would be considered beneficial as it reduces the availability of hydrophobic compounds to water and biota (32). Therefore, the faster aging of iron when palladized and slower dehalogenation kinetics with existence of AC should be taken into account when designing a "reactive capping barrier" for in-situ sediment or groundwater treatment of HHOCs with nZVI/Pd-AC. The inactivation of Pd over time due to its heterogeneous distribution on nZVI might further reduce the dehalogenation kinetics. Improvements in synthesis are needed to increase the overall fraction of zero-valent iron in nZVI/Pd-AC composites.

Supplementary Material

Refer to Web version on PubMed Central for supplementary material.

Acknowledgments

This work was supported by Superfund Research Program, National Institute of Health (R01ES1614). We thank Matthew A. Marcus and Peter S. Nico for assistance in conducting μXRF imaging and data processing o n beam line 10.3.2 at ALS. ALS is supported by the Department of Energy, Office of Basic Energy Sciences.

Literature Cited

1. Ghosh U, Zimmerman JR, Luthy RG. PCB and PAH speciation among particle types in contaminated harbor sediments and effects on PAH bioavailability. Environ. Sci. Technol. 2003; 37(10):2209–2217. [PubMed: 12785527]
2. Ciparis S, Hale RC. Bioavailability of polybrominated diphenyl ether flame retardants in biosolids and spiked sediment to the aquatic oligochaete, Lumbriculus variegatus. Environ. Toxicol. Chem. 2005; 24(4):916–925. [PubMed: 15839567]
3. Lowry GV, Johnson KM. Congener-specific dechlorination of dissolved PCBs by microscale and nanoscale zerovalent iron in a water/methanol solution. Environ. Sci. Technol. 2004; 38(19):5208–5216. [PubMed: 15506219]
4. Zhuang YA, Ahn S, Luthy RG. Debromination of polybrominated diphenyl ethers by nanoscale zerovalent iron: Pathways, kinetics, and reactivity. Environ. Sci. Technol. 2010; 44(21):8236–8242. [PubMed: 20923154]
5. Kim JH, Tratnyek PG, Chang YS. Rapid dechlorination of polychlorinated dibenzo-p-dioxins by bimetallic and nanosized zerovalent iron. Environ. Sci. Technol. 2008; 42(11):4106–4112. [PubMed: 18589973]
6. Zhu BW, Lim TT. Catalytic reduction of Chlorobenzenes with Pd/Fe nanoparticles: reactive sites, catalyst stability, particle aging, and regeneration. Environ. Sci. Technol. 2007; 41(21):7523–7529. [PubMed: 18044536]

7. Carvalho-Knighton, K.; Talalaj, L.; DeVor, R. Environmental Applications of Nanoscale and Microscale Reactive Metal Particles. Vol. 1027. American Chemical Society; 2009. PBDE degradation with zero-valent bimetallic systems; p. 75-87.
8. Choi H, Al-Abed SR, Agarwal S, Dionysiou DD. Synthesis of reactive nano-Fe/Pd bimetallic system-impregnated activated carbon for the simultaneous adsorption and dechlorination of PCBs. Chem. Mater. 2008; 20(11):3649–3655.
9. Zimmerman JR, Werner D, Ghosh U, Millward RN, Bridges TS, Luthy RG. Effects of dose and particle size on activated carbon treatment to sequester polychlorinated biphenyls and polycyclic aromatic hydrocarbons in marine sediments. Environ. Toxicol. Chem. 2005; 24(7):1594–1601. [PubMed: 16050574]
10. Ahn S, Werner D, Karapanagioti HK, McGlothlin DR, Zare RN, Luthy RG. Phenanthrene and pyrene sorption and intraparticle diffusion in polyoxymethylene, coke, and activated carbon. Environ. Sci. Technol. 2005; 39(17):6516–6526. [PubMed: 16190207]
11. Schrick B, Blough JL, Jones AD, Mallouk TE. Hydrodechlorination of trichloroethylene to hydrocarbons using bimetallic nickel-iron nanoparticles. Chem. Mater. 2002; 14(12):5140–5147.
12. Chun CL, Baer DR, Matson DW, Amonette JE, Penn RL. Characterization and reactivity of iron nanoparticles prepared with added Cu, Pd, and Ni. Environ. Sci. Technol. 2010; 44(13):5079–5085. [PubMed: 20509654]
13. Keum YS, Li QX. Reductive debromination of polybrominated diphenyl ethers by zerovalent iron. Environ. Sci. Technol. 2005; 39(7):2280–2286. [PubMed: 15871265]
14. Agarwal S, Al-Abed SR, Dionysiou DD, Graybill E. Reactivity of substituted chlorines and ensuing dechlorination pathways of select PCB congeners with Pd/Mg bimetallics. Environ. Sci. Technol. 2009; 43(3):915–921. [PubMed: 19245036]
15. Eberson, L. Electron Transfer Reactions in Organic Chemistry. Berlin, Germany: Springer-Verlag; 1987.
16. Xuan XL, Li XZ, Wang C, Liu H. Effects of key reaction parameters on the reductive dechlorination of chloroform with Pd/Fe^0 bimetal in aqueous solution. J. Environ. Sci. Health A-Tox./Hazard. Subst. Environ. Eng. 2010; 45(4):464–470.
17. Fang Y, Al-Abed SR. Correlation of 2-chlorobiphenyl dechlorination by Fe/Pd with iron corrosion at different pH. Environ. Sci. Technol. 2008; 42(18):6942–6948. [PubMed: 18853813]
18. Shih YH, Tai YT. Reaction of decabrominated diphenyl ether by zerovalent iron nanoplarticles. Chemosphere. 2010; 78(10):1200–1206. [PubMed: 20117822]
19. Cwiertny DM, Bransfield SJ, Roberts AL. Influence of the oxidizing species on the reactivity of iron-based bimetallic reductants. Environ. Sci. Technol. 2007; 41(10):3734–3740. [PubMed: 17547205]
20. Xu Y, Zhang WX. Subcolloidal Fe/Ag particles for reductive dehalogenation of chlorinated benzenes. Ind. Eng. Chem. Res. 2000; 39(7):2238–2244.
21. Devor R, Carvalho-Knighton K, Aitken B, Maloney P, Holland E, Talalaj L, Elsheimer S, Clausen CA, Geiger CL. Mechanism of the degradation of individual PCB congeners using mechanically alloyed Mg/Pd in methanol. Chemosphere. 2009; 76(6):761–766. [PubMed: 19535124]
22. Kim YH, Shin WS, Ko SO. Reductive dechlorination of chlorinated biphenyls by palladized zero-valent metals. J. Environ. Sci. Health A-Tox./Hazard. Subst. Environ. Eng. 2004; 39(5):1177–1188.
23. Li A, Tai C, Zhao ZS, Wang YW, Zhang QH, Jiang GB, Hu JT. Debromination of decabrominated diphenyl ether by resin-bound iron nanoparticles. Environ. Sci. Technol. 2007; 41(19):6841–6846. [PubMed: 17969704]
24. Noma Y, Ohno M, Sakai S. Pathways for the degradation of PCBs by palladium-catalyzed dechlorination. Fresenius Environ. Bull. 2003; 12(3):302–308.
25. Coburn CG, Curras-Collazo MC, Kodavanti PRS. Polybrominated diphenyl ethers and ortho-substituted polychlorinated biphenyls as neuroendocrine disruptors of vasopressin release: Effects during physiological activation in vitro and structure-activity relationships. Toxicol. Sci. 2007; 98(1):178–186. [PubMed: 17434953]
26. Meerts I, Letcher RJ, Hoving S, Marsh G, Bergman A, Lemmen JG, van der Burg B, Brouwer A. In vitro estrogenicity of polybrominated diphenyl ethers, hydroxylated PBDEs, and

polybrominated bisphenol A compounds. Environmental Health Perspectives. 2001; 109(4):399–407. [PubMed: 11335189]

27. Alonso F, Beletskaya IP, Yus M. Metal-mediated reductive hydrodehalogenation of organic halides. Chem. Rev. 2002; 102(11):4009–4091. [PubMed: 12428984]
28. Feng J, Lim TT. Iron-mediated reduction rates and pathways of halogenated methanes with nanoscale Pd/Fe: Analysis of linear free energy relationship. Chemosphere. 2007; 66(9):1765–1774. [PubMed: 16899274]
29. Yak HK, Lang QY, Wai CM. Relative resistance of positional isomers of polychlorinated biphenyls toward reductive dechlorination by zerovalent iron in subcritical water. Environ. Sci. Technol. 2000; 34(13):2792–2798.
30. Choi H, Al-Abed SR, Agarwal S. Catalytic role of palladium and relative reactivity of substituted chlorines during adsorption and treatment of PCBs on reactive activated carbon. Environ. Sci. Technol. 2009; 43(19):7510–7515. [PubMed: 19848169]
31. Choi H, Al-Abed SR. Effect of reaction environments on the reactivity of PCB (2-chlorobiphenyl) over activated carbon impregnated with palladized iron. J. Hazard. Mater. 2010; 179(1–3):869–874. [PubMed: 20388583]
32. Cho YM, Ghosh U, Kennedy AJ, Grossman A, Ray G, Tomaszewski JE, Smithenry DW, Bridges TS, Luthy RG. Field application of activated carbon amendment for in-situ stabilization of polychlorinated biphenyls in marine sediment. Environ. Sci. Technol. 2009; 43(10):3815–3823. [PubMed: 19544893]

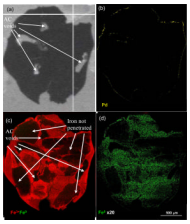

Figure 1.
Optical (a) and micro X-ray fluorescence images (b–d) of an nZVI/Pd-AC particle thin section showing distribution of Pd indicated in yellow (b), a Fe^{3+}-Fe^{0} speciation image plotted on the same intensity scale (c), and the distribution of Fe^{0} with signal intensity increased 20 times that of Fe^{3+}. Brighter color indicates higher abundance.

Table 1

Physical and Chemical Properties of Particles.

	Particle size	N_2 BET surface area (m^2/g)	Pore size (cm^3/g)	Elemental composition (wt %)			
				Fe_t	Fe^0	Pd	B
nZVI[a]	50–70 nm	16±1	-	76±2	55±3	-	5±1
nZVI/Pd	20–50 nm	36±1	-	76±2	55±5	0.25±0.02	5±1
AC	0.6–2 mm	610±7	0.582±0.04	-	-	-	-
nZVI/Pd-AC	0.6–2 mm	333±10	0.312±0.02	14±2	1±0.2	0.30±0.02	0.5
RAC[b]	0.85–2 mm	358	0.352	14.4	-	0.68	-

[a] Zhuang, et al. (4)

[b] Choi, et al. (8)

Table 2

Debromination rate constants and half-life of selected PBDEs and PCB 21 by nZVI/Pd, nZVI and nZVI/Pd-AC.

Particle	O_2 content [ppm]	IUPAC No.	PBDE/PCB congener	k_{obs} [1/d]	k_{Fe} [a] [L/d·g]	k_{Pd} [b] [L/d·g]	Half-life [d]
nZVI/Pd	~7.8	BDE 1	2-monoBDE	0.38	6.91 E-02	15.2	1.82
		BDE 2	3-monoBDE	1.28	2.33 E-01	51.2	0.54
		BDE 3	4-monoBDE	1.37	2.49 E-01	54.8	0.51
		BDE 8	2,4'-diBDE	1.70	3.09 E-01	68.0	0.41
		BDE 12	3,4-diBDE	1.59	2.89 E-01	63.6	0.44
		BDE 28	2,4,4'-triBDE	3.02	5.29 E-01	121	0.23
		BDE 33	2,3',4'-triBDE	2.72	4.95 E-01	109	0.25
		BDE 21	2,3,4-triBDE	2.43	4.42 E-01	97.2	0.29
		PCB 21	2,3,4-triCB	9.90 E-02	1.80 E-02	3.97	7.00
nZVI/Pd	~0.5	BDE 8	2,4'-diBDE	7.80	1.42	211	0.09
		BDE 12	3,4-diBDE	6.56	1.19	177	0.11
		BDE 33	2,3',4'-triBDE	8.04	1.46	217	0.09
nZVI[c]	~7.8	BDE 1	2-monoBDE	2.80 E-03	5.09 E-05	-	247
		BDE 2	3-monoBDE	3.40 E-03	6.18 E-05	-	203
		BDE 3	4-monoBDE	2.70 E-03	4.91 E-05	-	256
		BDE 12	3,4-diBDE	3.14 E-02	5.72 E-04	-	22
		BDE 21	2,3,4-triBDE	2.95 E-01	5.37 E-03	-	2.35
		PCB 21	2,3,4-triCB	2.00 E-03	3.64 E-05	-	347
nZVI/Pd-AC	~7.8	BDE 21	2,3,4-triBDE	5.00 E-02	5.00 E-01	2.02	13.9
	<0.1	PCB 21[d]	2,3,4-triCB	4.27 E-01	2.97 E-02	0.61	1.62

[a] The observed rate constants (k_{obs}) were normalized by the mass concentration of ZVI.

[b] The observed rate constants (k_{obs}) were normalized by the mass concentration of Pd if applicable.

[c] Zhuang, et al. (4)

[d] Choi, et al. (30)

Table 3

Effect of oxygen content on apparent rates of hydrogen production (corrosion rate) by 1 g nZVI (2 weeks) or 0.1 g nZVI/Pd (2 days) exposure to 10 ml acetone/water (50:50, v/v) solution. The set up is the same as that for the debromination tests.

Particles	O_2 content [ppm]	H_2 production rate	
		[mmol/kgFe^0/d]	[mmol /d]
nZVI/Pd	~7.8	3478.7	1.91 E-01
nZVI/Pd	~0.5	4220.8	2.32 E-01
nZVI	~7.8	35.4	1.95 E-02
nZVI	~0.5	41.1	2.26 E-02